

## ENTROPY VISCOSITY FOR CONSERVATION EQUATIONS

J.L. Guermond<sup>†</sup>, R. Pasquetti<sup>\*</sup> and B. Popov<sup>††</sup>

<sup>\*</sup>Lab. J.A. Dieudonné, UMR CNRS 6621, UNS  
06108, Nice, France

e-mail: richard.pasquetti@unice.fr

<sup>††</sup>Dpt of Mathematics, Texas A & M University  
College-Station, USA

e-mail: {guermond,popov}@math.tamu.edu

**Key words:** Fluid Dynamics, conservation laws, stabilization methods, entropy viscosity.

**Abstract.** *We present an “entropy viscosity method” for the approximation of conservation laws and more generally of conservation equations or systems that may exhibit non-smooth solutions. To emphasize its capabilities we focus on some non-trivial problems, governed by non-linear scalar conservation laws or by the compressible Euler equations. Numerical results obtained with finite elements, Fourier spectral method and spectral elements are provided to outline the fact that different types of approximations may be used. We also consider the linear scalar advection equation, that we solve with spectral elements, to provide a numerical evidence that the accuracy of the underlying method is preserved. This stabilization method is based on the introduction in the governing equations of a non-linear stabilizing term, which makes use of a non-linear viscosity constructed from the residual of the entropy equation associated to the considered problem.*

### 1 Introduction

We are interested in the solution of stiff problems, *e.g.* obtained when nonlinear hyperbolic equations are considered, so that shocks may develop. Such problems may also occur when turbulent flows are concerned, since in this case the computational grid is generally too coarse to resolve the smallest scales of the flow. This topic is of course not new, especially in the frame of finite volume methods for conservation laws: Monotone or TVD (Total Variation Diminishing) schemes have motivated many researches in order to enhance the accuracy far from the shocks together with a non-oscillatory behavior at the shocks. This is mainly based on the use of flux / slope limiters, which provide an upper bound for the fluxes, and ENO (Essentially Non Oscillatory) type polynomial reconstructions. Such approaches are however rather complex, difficult to extend to different types of approximations and generally computationally expensive. One may consult [8] for an overview of such approaches.

Standard numerical methods, like the Finite Element Method (FEM), generally fail to handle such stiff problems. This is especially true for high order methods, like the Fourier spectral method, as a result of the well known Gibbs phenomenon. However, when taking into account that nonlinear schemes with flux / slope limiters essentially consist of adding some *nonlinear viscosity dissipation*, one may think to complement the Partial Differential Equation (PDE) with an additional dissipation term. This reminds of course the Von Neumann - Richtmayer approach [14], developed 60 years ago, which is well known to be too diffusive. To preserve the accuracy of the underlying numerical method, the additional dissipation must at least be localized. In the frame of spectral methods, the so-called “spectral (vanishing) viscosity” technique [13] consists of introducing some dissipation in the high frequency range of the spectral approximation. This approach, localized in spectral space, is however essentially linear. Using a Discontinuous Galerkin *hp*-FEM approximation, the authors in [11] recently proposed to introduce a dissipation term localized in physical space and based on a viscosity controlled by a smoothness indicator. For us we also suggest to introduce some dissipation where strong gradients form. To this end, we have proposed to construct a nonlinear viscosity based on the residual of the entropy equation associated to the considered PDE (or system). Such an approach, based on a strong physical background, was first applied to the Fourier approximation of the inviscid Burgers equation and to the 1D Euler system with very satisfactory results [5]. Recently the method was revisited [6, 7], using a simplified formulation, and 2D problems were investigated using other kind of approximations.

Here we want to outline that the Entropy Viscosity (EV) method can be implemented using various numerical approximations and also that the method preserves the approximation order. In Section 2, the basic formulation of the EV method is described. In Section 3, we solve a nonlinear scalar conservation law with the Spectral Element Method (SEM) and also consider the linear advection equation to show that the present stabilization method preserves the approximation order. In Section 4, we address a 2D Burgers problem as well as the Euler system with the Fourier approximation. Finally, different results obtained with the FEM for flows governed by the compressible Euler equations are presented.

## 2 The entropy viscosity method

The relevant weak solution of the *scalar* conservation law

$$\partial_t u(\vec{x}, t) + \nabla \cdot \vec{f}(u(\vec{x}, t)) = 0, \quad \vec{x} \in \Omega, \quad t \in \mathbb{R}^+ \quad (1)$$

with appropriate initial and boundary conditions, is the so-called entropy solution, which is also characterized by  $u = \lim_{\nu \rightarrow 0} u_\nu$  where

$$\partial_t u_\nu + \nabla \cdot \vec{f}(u_\nu) = \nu \Delta u_\nu. \quad (2)$$

Starting from this point, the EV method introduces a nonlinear dissipation term  $\nabla \cdot (\nu_h \nabla u)$  in the right hand side of (1), where  $\nu_h$  is a local artificial nonlinear viscosity set up from

the residual of the entropy equation.

Let  $E(u)$  be a convex function and assume that there exists an entropy pair  $(E(u), \vec{F}(u))$  such that

$$\partial_t E(u) + \nabla \cdot \vec{F}(u) \leq 0$$

characterizes the unique viscous limit to (1) (*i.e.* the entropy solution). Let  $r_E(u) := \partial_t E(u) + \nabla \cdot \vec{F}(u)$  be the entropy residual. This quantity is a negative measure supported on the shocks, *i.e.*  $r_E < 0$  at the shocks and  $r_E = 0$  elsewhere.

Assume that the computational domain  $\Omega$  is discretized, let  $h$  be the grid size and  $u_h$  the numerical solution. We propose to construct a local viscosity based on the entropy residual  $r_E(u_h)$ . First we set

$$\nu_E(\vec{x}, t) := \alpha_E h^2(\vec{x}) \mathcal{R}(r_E(u_h)) / \|E(u_h) - \bar{E}\|_{\infty, \Omega} \quad (3)$$

where  $\alpha_E$  is a proportionality coefficient,  $\bar{E}$  is the space average of  $E(u_h)$  (recall that  $E$  is defined up to a constant),  $\|\cdot\|_{\infty, \Omega}$  is the usual  $L^\infty(\Omega)$  norm and  $\mathcal{R}(r_E)$  is a positive function (or functional) of the residual  $r_E$ . The terms  $h^2(\vec{x})$  and  $\|E(u_h) - \bar{E}\|_{\infty, \Omega}$  are scaling factors. The aim of  $\mathcal{R}(r_E)$  is to extract a useful information from the residual, *e.g.*  $\mathcal{R}(r_E) = |r_E|$ . Note that in smooth parts of  $u$ , one may expect that  $r_E(u_h)$  scales like the approximation error of the solution method.

Let us now provide an upper bound for the entropy viscosity. For the one-dimensional scalar conservation equation  $\partial_t u + f'(u) \partial_x u = 0$ , the first-order Finite Difference upwind scheme (linear monotone scheme) is equivalent to the second-order centered Finite Difference approximation augmented with a viscous dissipation with viscosity  $\nu_{max} = 0.5 f'(u) h$ . By analogy we set

$$\nu_{max}(\vec{x}, t) = \alpha_{max} h \max_{\vec{y} \in V_{\vec{x}}} |f'(u_h(\vec{y}, t))|, \quad (4)$$

where  $\alpha_{max}$  is a constant coefficient, and  $V_{\vec{x}}$  is a neighborhood of  $\vec{x}$  still to be defined and dependent on the approximation method. In practice the size of  $V_{\vec{x}}$  is a few multiples of  $h$  in each direction. Finally the entropy viscosity is defined to be

$$\nu_h(\vec{x}, t) := \mathcal{S}(\min(\nu_{max}, \nu_E)) \quad (5)$$

where  $\mathcal{S}$  is a smoothing operator. Smoothing may indeed be required because  $r_E(u_h)$  is generally highly oscillatory, since we actually try to approximate a Dirac distribution when a shock occurs. Practical implementation details on the operators  $\mathcal{R}$ ,  $\mathcal{S}$  and on the neighborhood  $V_{\vec{x}}$ , as well as details on how to tune the coefficients  $\alpha_E$  and  $\alpha_{max}$  are provided in the examples studied in next sections.

### 3 SEM approximation

We begin these numerical tests with the SEM approximation. First we consider a non-linear scalar conservation law, the KPP rotating wave, as initially proposed by Kurganov, Petrova and Popov [4]. Then we consider a linear transport problem to check that the

spectral accuracy is preserved, as could be expected since the viscosity is based on a residual. For the SEM approximation we use  $\mathcal{R}(r_E) = |r_E|$ .

### 3.1 KPP rotating wave (SEM)

We solve the nonlinear scalar conservation law:

$$\partial_t u + \nabla \cdot \vec{f}(u) = 0, \quad \vec{f}(u) = (\sin u, \cos u)$$

$0 < t \leq 1$ ,  $\vec{x} \in (-2, 2) \times (-2.5, 1.5)$ , with the initial condition:

$$u|_{t=0} = 3.5\pi \quad \text{if } |\vec{x}| < 1 \quad u|_{t=0} = \pi/4 \quad \text{elsewhere.}$$

For this problem the local velocity is such that:  $\vec{v} = \vec{f}'(u) = (\cos u, -\sin u)$ . To implement the EV method one must define an entropy pair. We choose:

$$E(u) = u^2/2, \quad \vec{F}(u) = (u \sin u + \cos u, u \cos u - \sin u). \quad (6)$$

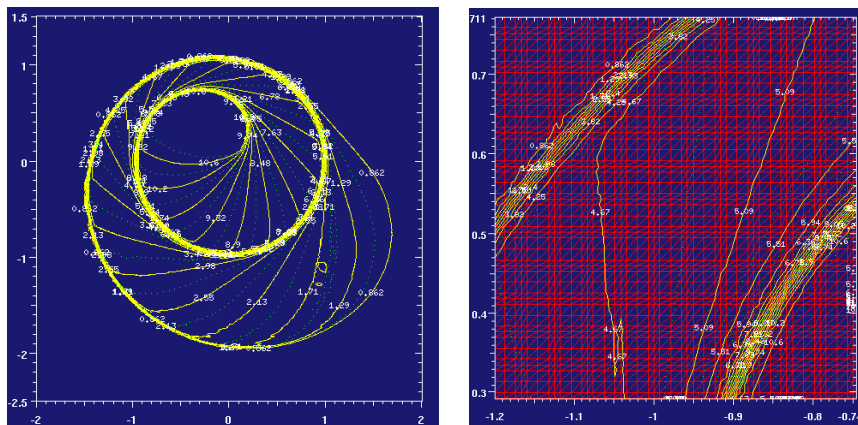


Figure 1: SEM - RK4 solution of the KPP rotating wave (at left) and zoom (at right) together with the SEM mesh (diagonals of the mesh are meaningless);  $N = 4$ ,  $n = 96^2$ .

The domain is uniformly discretized using squares of side  $h$  and the approximation space is composed of the functions that are continuous and piecewise polynomial of partial degree at most  $N$ . The local shape functions are the Lagrange polynomials associated with the  $(N + 1)^2$  Gauss-Lobatto-Legendre (GLL) points. To define the entropy viscosity we follow the procedure described in Section 2, except that in (4) we have used the local grid size of the Gauss-Lobatto-Legendre (GLL) mesh, say  $h_{GLL}$ , rather than  $h$ . The neighborhood  $V_{\vec{x}}$  is defined as the corresponding spectral element of  $\vec{x}$ , during the assembling procedure. The smoothing is achieved inside each element on the GLL mesh, by one smoothing sweep based on a two-dimensional averaging rule involving 5 GLL grid-points. The EV control parameters are  $\alpha_E = 40$  and  $\alpha_{max} = 0.8/N$ . The time marching

is done by using the standard Runge-Kutta scheme (RK4). The entropy viscosity is made explicit and computed by using the second order backward finite difference approximation for the time derivative of the entropy.

Results are provided in Fig. 1, as obtained with the standard SEM using a regular mesh of  $n = 96^2$  spectral elements with a polynomial approximation degree  $N = 4$  in each of them. At left, the numerical solution shows the expected rotating shock wave structure. At right, we focus on a part of the figure and visualize the spectral element mesh.

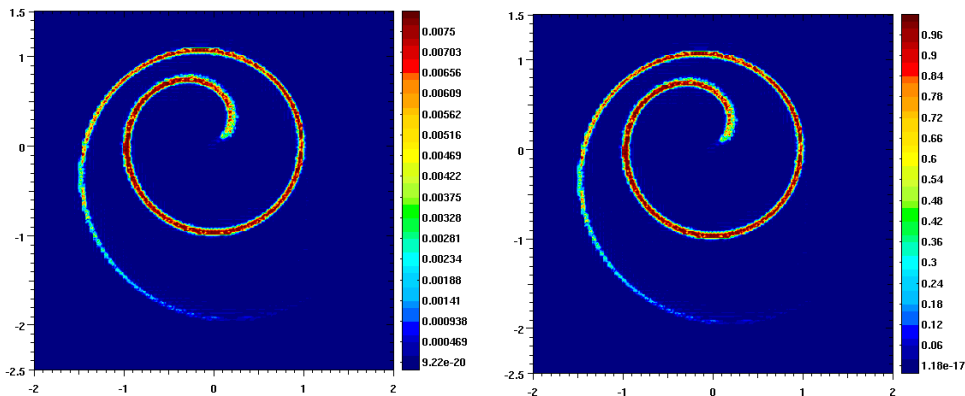


Figure 2: SEM - RK4 solution of the KPP rotating wave: Visualization of the entropy viscosity  $\nu_h$  and of the entropy ratio  $\nu_h/\nu_{max}$ ;  $N = 4$ ,  $n = 96^2$ .

We now give details on the way the EV parameters are adjusted. The idea is that to be efficient, the viscosity must reach its maximum value at the shocks. Consequently, we follow the two-step adjustment procedure:

1. Set  $\alpha_E = \infty$  and increase  $\alpha_{max}$  till obtaining a smooth solution.
2. Set  $\alpha_{max}$  fixed and increase  $\alpha_E$  till the entropy viscosity saturates at the shocks, so that  $\max(\nu) = \nu_{max}$ .

In Fig. 2 (left) the entropy viscosity is visualized. As expected, dissipation is added exactly where the shock develops. In Fig. 2 (right), the viscosity ratio  $\nu_h/\nu_{max}$  is visualized. As desired, this ratio equals 1 at the shock.

Such a tuning procedure is not specific to the SEM and so is systematically applied in all forthcoming test cases.

### 3.2 Rotating transport (SEM)

To point out the properties of the method, we focus now on the following classical transport problem: advection, in the domain  $(-1, 1)^2$  by a velocity corresponding to a

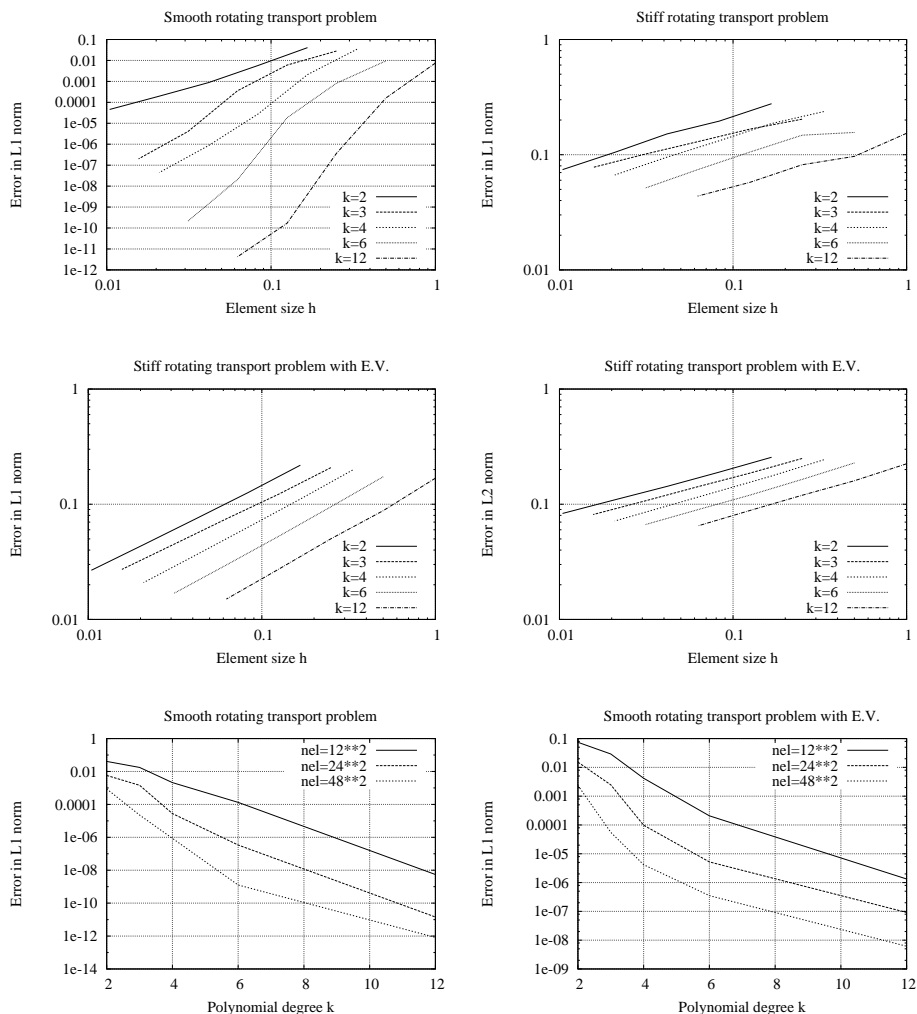


Figure 3: Up: Errors for the smooth (at left) and stiff rotating transport problems (at right) with SEM. Middle: Errors for the stiff rotating transport problem in  $L^1$  (at left) and  $L^2$  norms (at right) with entropy viscosity. Down:  $L^1$ -errors for smooth rotating transport problem with pure Galerkin (at left) and viscosity entropy solutions (at right)

solid rotation, *i.e.*  $\vec{f}(u) = u\vec{v}$ ,  $\vec{v} = 2\pi\rho(-\sin\theta, \cos\theta)$ , where  $(\rho, \theta)$  are the cylindrical coordinates. Two cases are considered: In the first case the initial condition is the characteristic function of the disc of radius  $r_0 = 0.3$  centered at  $(\rho = 0.4, \theta = 0)$ ; In the second case, the initial data is the function  $0.5(1 - \tanh(\delta^2/r_0^2 - 1))$ , where  $\delta$  is the distance to the disc center. Correspondingly we refer to the smooth or the stiff “rotating transport” problems.

### 3.2.1 Accuracy study

Pure Galerkin SEM solutions of the smooth and stiff rotating transport problems have first been computed. Of course, in the stiff case the Galerkin solution oscillates. The corresponding errors, with respect to the spectral element size and measured after one rotation, are given in Fig. 3 (top). Clearly, for the smooth problem the errors are quickly decreasing, the convergence rate depending on the polynomial approximation degree  $N$  in each spectral element, whereas, as expected, for the stiff problem the convergence rate is close to 0.5 in  $L^1$  norm.

Computations have been carried out with the EV method. The smoothing operator is implemented at the level of each spectral element, by using a local mean value obtained through a 5 GLL points quadrature, based on the trapezoidal rule. Computations have been carried out with  $\alpha_E = 2$  and  $\alpha_{max} = 0.05/N$ , without trying to fine tune these parameters. The errors, both in  $L^1$  and  $L^2$  norms are given in Fig. 3 (center). The solution is now smooth and improved convergence rates are obtained, *i.e.*, close to 1 in  $L^1$  norm and 0.5 in  $L^2$  norms. Such values are the maxima that can be expected.

Since the entropy viscosity is set up from a residual, one may check that the EV method preserves the spectral accuracy. Thus, Fig. 3 (bottom) shows that when considering the smooth rotating transport problem the convergence rate with respect to the polynomial degree remains exponential. However, as could be expected the rate is slightly lower than for the pure SEM approximation.

### 3.2.2 Long time behavior

To study the long time behavior of the solution, computations have been made until time  $t = 100$ , *i.e.* after one hundred loops. These computations have been made for the stiff transport problem, using the pure Galerkin approach or Galerkin plus the EV stabilization. Moreover, various polynomial approximation degrees have been used:  $N = \{2, 3, 4, 6, 12\}$ , keeping constant the number of degrees of freedom (dof=14641).

Results are shown in Fig. 4, where projections of 3D visualizations are provided. Clearly, the pure Galerkin solution is affected with wild oscillations whereas the EV solution is smooth. However, the EV solution has diffused for low order polynomial. On the contrary, it still remains stiff for high values of  $N$ . This shows that high order methods are well suited for pure transport problems when associated to a nonlinear stabilization like the EV method.

## 4 Fourier approximation

Even if the Fourier approximation is a *a priori* not the good choice for conservation laws, we show in this Section that valuable results may be obtained when the entropy viscosity is implemented. First we consider a 2D Burgers problem for which we can provide numerical convergence results. Then we address the Euler system and consider a classical

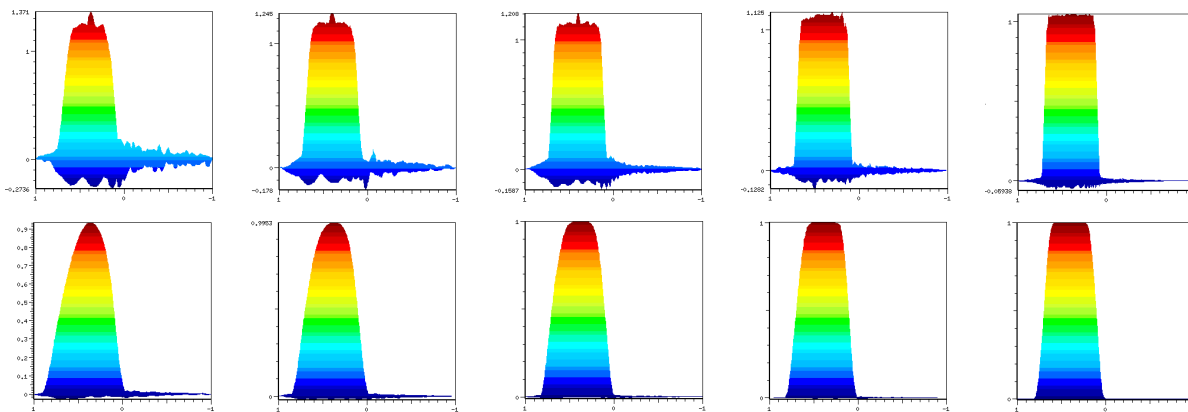


Figure 4: From left to right: Solutions for the stiff rotating transport problem after 100 loops for different polynomial degrees  $N = \{2, 3, 4, 6, 12\}$ . First line: Pure Galerkin; Second line: with EV stabilization.

test used to compare different numerical methods. Here again we use  $\mathcal{R}(r_E) = |r_E|$ .

#### 4.1 2D Burgers

Using Fourier expansions, we want to solve the inviscid Burgers equation:

$$\partial_t u + \nabla \cdot \left( \frac{u^2}{2} \vec{v} \right) = 0, \quad \vec{v} = (1, 1)$$

$0 < t \leq 0.5$ ,  $\vec{x} \in (0, 1)^2$ , with a piecewise constant initial condition. Constant values are thus assigned in the four quadrants separated by  $x = 0.5$  and  $y = 0.5$ : From up to down and left to right,  $u|_{t=0} = \{-0.2, -1., 0.5, 0.8\}$

The local velocity is here  $\vec{f}'(u) = u\vec{v}$ , *i.e.* the velocity is parallel to  $\vec{v}$  and its amplitude equals  $u$ .

To solve such a problem with Fourier expansions one must first set up a periodic problem. This is simply done by considering the computational domain  $(0, 2)^2$ , the initial condition being extended by symmetry with respect to  $x = 1$ ,  $y = 1$ .

For the entropy pair we choose  $(E(u) = u^2/2, \vec{F}(u) = u^3\vec{v}/3)$  and then again follow the procedure described in Section 2. The smoothing is simply achieved through a double sweep, each one consisting of a 5 point mean value based on the trapezoidal rule. The local maximum of the velocity is obtained within a  $7 \times 7$  local grid.

Computation were done with 192 Fourier modes in each direction and de-aliasing, *i.e.* with  $192^2$  grid points in  $(0, 1)^2$ . For the EV control parameters we used  $\alpha_E = 0.2$  and  $\alpha_{max} = 1.5$ . Results are given in Fig. 5 (at left), showing that the shock is well captured. The zoom, in Fig. 5 (at right), shows the underlying mesh. Note that since we are using the 3/2 de-aliasing rule, the effective grid is 3/2 coarser than the one visualized.

For the considered 2D inviscid Burgers problem one can determine an exact solution, so that it is possible to provide some convergence results. Table 1 provides the errors between

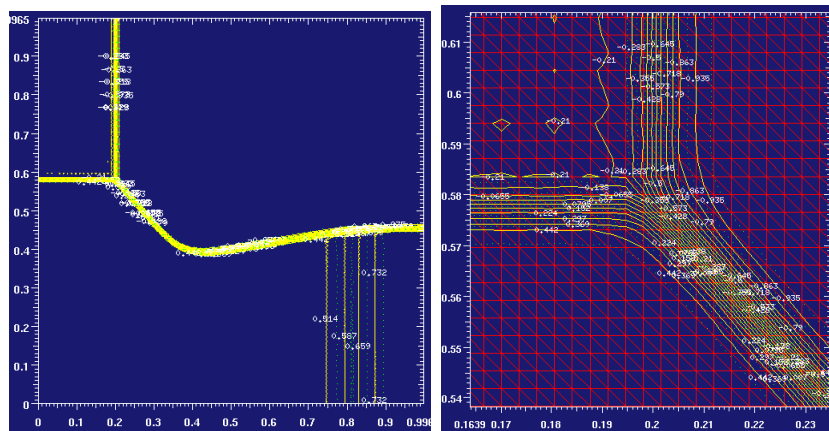


Figure 5: Fourier-RK4 solution of the 2D Burgers problem (at left) and detail of the mesh (at right) (diagonals of the mesh are meaningless).

Table 1: Errors and convergence rates for the 2D Burgers problem.

h	$L^1$	rate	$L^2$	rate
2.78E-2	1.92E-2	–	1.02E-1	–
1.39E-2	9.99E-3	0.94	7.28E-2	0.49
6.94E-3	5.34E-3	0.89	5.41E-2	0.43
3.47E-3	2.79E-3	0.95	3.80E-2	0.51

the exact and numerical solutions for different grid sizes as well as the convergence rates, both in  $L^1$  and  $L^2$  norms. One clearly observe convergence rates close to the maxima that can be expected, *i.e.* 1 in  $L^1$  norm and 0.5 in  $L^2$  norm.

## 4.2 2D Euler system

Here we show how the EV method can be adapted to the compressible Euler equations:

$$\partial_t \vec{u} + \nabla \cdot \vec{f}(\vec{u}) = 0, \quad \vec{u} = \begin{pmatrix} \rho \\ \rho \vec{v} \\ E \end{pmatrix}, \quad \vec{f} = \begin{pmatrix} \rho \vec{v} \\ \rho \vec{v} \otimes \vec{v} + p \mathbb{I} \\ \vec{v}(E + p) \end{pmatrix} \quad (7)$$

where  $p = \rho T$ ,  $T = (\gamma - 1)(E/\rho - \vec{v}^2/2)$ . Usual notations are used:  $\rho, \vec{v}, p, T, \gamma, E$  stand for density, velocity, pressure, temperature, ratio of specific heat, and total energy, respectively. The physical entropy functional

$$S(p, \rho) = \frac{\rho}{\gamma - 1} \log(p/\rho^\gamma)$$

is such that  $r_S := \partial_t S + \nabla \cdot (\vec{v}S) \geq 0$ .

To understand where and how the entropy dissipation must be set, it is helpful to follow the physics by considering the viscous fluxes appearing in the Navier-Stokes equations:

$$\vec{f}_{visc}(\vec{u}) = \begin{pmatrix} 0 \\ -\mu \nabla \vec{v} \\ -\mu \nabla \frac{v^2}{2} - \kappa \nabla T \end{pmatrix}.$$

The quantity  $\mu$  is the dynamic viscosity and  $\kappa$  is the thermal conductivity.

First, we compute  $\mu_E$ , except that there is no need to normalize by  $\|S - \bar{S}\|_{\infty, \Omega}$  in (5):

$$\mu_E = \alpha_E h^2 \rho(\vec{x}, t) |r_S(\vec{x}, t)|.$$

Then, estimating the maximum local wave speed to be  $|\vec{v}| + \sqrt{\gamma T}$ , we set

$$\mu_{max} = \alpha_{max} h \rho(\vec{x}, t) \max_{\vec{y} \in V_{\vec{x}}} (|\vec{v}(\vec{y}, t)| + \sqrt{\gamma T(\vec{y}, t)}).$$

Finally,

$$\mu_h = \mathcal{S}(\min(\mu_{max}, \mu_E))$$

and, taking  $\kappa_h$  to be proportional to  $\mu_h$ :  $\kappa_h = \mathcal{P} \mu_h$ .

We now validate this approach by solving the benchmark problem number 12 from [9]. It is a two-dimensional Riemann problem set in  $\mathbb{R}^2$ . In the restricted computational domain  $(0, 1)^2$  the initial set of data is defined as follows:

$$\begin{array}{llll} p = 1., & \rho = 0.8, & \vec{v} = (0., 0.), & 0. < x < 0.5 \quad 0. < y < 0.5, \\ p = 1., & \rho = 1., & \vec{v} = (0.7276, 0.), & 0. < x < 0.5, \quad 0.5 < y < 1., \\ p = 1., & \rho = 1., & \vec{v} = (0., 0.7276), & 0.5 < x < 1., \quad 0. < y < 0.5, \\ p = 0.4, & \rho = 0.5313, & \vec{v} = (0., 0.) & 0.5 < x < 1., \quad 0.5 < y < 1.. \end{array}$$

The solution is computed at time  $t = 0.2$ . Proceeding as in Section 4.1, the problem is first made periodic by extending the computational domain to  $(0, 2)^2$ , and the initial data are extended by symmetry about the axes  $\{x = 1\}$  and  $\{y = 1\}$ .

The time marching algorithm, the definition of the smoothing operator, and the neighborhood  $V_{\vec{x}}$  are the same as in Section 4.1. The nonlinear terms are de-aliased. The control parameters for the entropy viscosity are  $\alpha_E = 20$ ,  $\alpha_{max} = 0.5$  and  $\mathcal{P} = 2$ . We show in Fig. 6 results obtained with 400 Fourier modes in each direction, *i.e.* with 400 grid-points in  $(0, 1)^2$ . They compare well with those obtained with other more sophisticated shock capturing methods, see [9].

## 5 FEM approximation

Examples based on the FEM approximation are considered in this Section. Here we use  $\mathcal{R}(r_E) = \|r_E\|_{\infty, K}$  where  $K$  denotes a generic element of the FEM mesh. Moreover

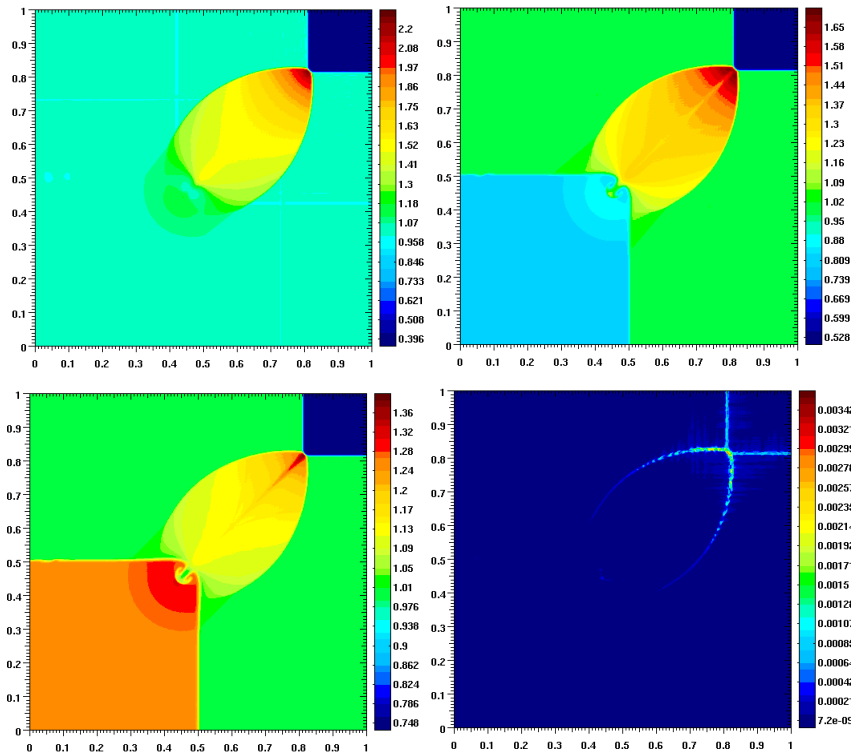


Figure 6: Fourier-RK4 solution of the Euler system: Pressure (top left); Density (top right); Temperature (bottom left); Entropy viscosity  $\mu_h$  (bottom right).

no smoothing is applied, the entropy viscosity  $\nu_h$  being taken constant on each element  $K$ . Tests for scalar conservation laws were provided in [7]. Here we focus on the Euler system and provide results for three challenging benchmarks. All these numerical tests have been done by using the explicit SSP RK3 time integration.

Similarly to the Fourier approximation, the algorithm consists of introducing an artificial viscosity and an artificial thermal diffusivity in the spirit of the Navier-Stokes equations. But at variance with the Fourier technique some stabilization is sometimes needed in the mass conservation equation. The viscous flux vector is defined to be as follows

$$\vec{f}_{visc} = \begin{pmatrix} -\nu_h \nabla \rho_h \\ -\mu_h \nabla \vec{v}_h \\ -\mu_h \nabla (\vec{v}_h^2)/2 - \kappa_h \nabla T_h \end{pmatrix}. \quad (8)$$

The algorithm is the following: At each time step we evaluate the residuals of the entropy equation and compute the associated artificial viscosities, then we update the mass, momentum, and total energy.

More specifically, for each mesh cell  $K$  the dynamic viscosity is computed as follows:

$$r_{h,1} := \partial_t S_h + \nabla \cdot (\vec{v}_h S_h), \quad (9)$$

$$r_{h,2} := \rho_h^{-1} S_h (\partial_t \rho_h + \nabla \cdot (\vec{v}_h \rho_h)), \quad (10)$$

$$\mu_E|_K := \alpha_E \|\rho_h\|_{\infty,K} h_K^2 \max(\|r_{h,1}\|_{\infty,K}, \|r_{h,2}\|_{\infty,K}). \quad (11)$$

The second residual  $r_{h,2}$  is meant to account for inaccuracies in mass conservation. Note that controlling  $r_{h,2}$  and  $r_{h,1}$  amounts to controlling the residual of the specific entropy,  $s_h := \rho_h^{-1} S_h$ , since

$$|\rho_h(\partial_t s_h + \vec{v}_h \cdot \nabla s_h)| = |r_{h,1} - r_{h,2}| \leq |r_{h,1}| + |r_{h,2}|.$$

The maximum dynamic viscosity,  $\mu_{\max}$ , is evaluated as follows:

$$\mu_{\max}|_K = \alpha_{max} h_K \|\rho_h\|_{\infty,K} (\|\vec{v}_h\| + \sqrt{\gamma T_h})_{\infty,K}. \quad (12)$$

Finally we set:

$$\mu_h = \min(\mu_{\max}, \mu_E), \quad \kappa_h = \frac{\mathcal{P}}{\gamma - 1} \mu_h, \quad \nu_h = \frac{\mathcal{P}_\rho}{\|\rho_h\|_{\infty,K}} \mu_h, \quad (13)$$

where  $\mathcal{P} \approx 1$  and  $\mathcal{P}_\rho \approx 1$ .

### 5.1 Mach 3 step

We illustrate the algorithm described above by considering the Mach 3 flow in a wind tunnel with a forward facing step. The geometry of the domain is shown in Figure 7. The initial data and inflow boundary conditions are specified in terms of the primitive variables

$$\left. \begin{aligned} &(\rho, \vec{v}, p)^T(x, y, 0) \\ &(\rho, \vec{v}, p)^T(0, y, t) \end{aligned} \right\} = (1.4, (3.0, 0.0), 1.0)^T. \quad (14)$$

The outflow boundary at  $\{x = 3\}$  is free. The slip condition  $\vec{v} \cdot \vec{n} = 0$  is specified on the solid wall of the tunnel,  $\vec{n}$  being the unit outward normal on  $\partial\Omega$ . This benchmark test has been proposed in [1] and has been popularized by Woodward and Colella's extensive study [15].

We show in Figure 7 the density field at  $t = 4$  on two different meshes with  $\mathbb{P}_1$  Lagrange finite elements. The results shown in the left panels have been obtained on a mesh composed of 4813  $\mathbb{P}_1$  nodes and the results shown in the right panels have been obtained on a mesh composed of 324927  $\mathbb{P}_1$  nodes. These computations have been done with  $\alpha_{max} = 0.25$ ,  $\alpha_E = 1$ ,  $\mathcal{P} = 0.1$  and  $\mathcal{P}_\rho = 0.1$ . The tests have been run with CFL = 0.5. Our solutions agree, at least qualitatively, with other reference solutions that can be found in the literature. The contact discontinuity emerging from the three-shock interaction

point is present in both simulations and is captured quite accurately. A Kelvin-Helmholtz instability develops along the contact discontinuity on the refined mesh.

As reported in [15] we have observed that the way the velocity boundary condition is implemented in the vicinity of the corner of the step somewhat influences the quality of the solution. We do not enforce any boundary condition at the node at the corner of the step in the computation, enforcing the slip condition at this particular point implies  $\vec{v} = 0$ , which is too strong a constraint.

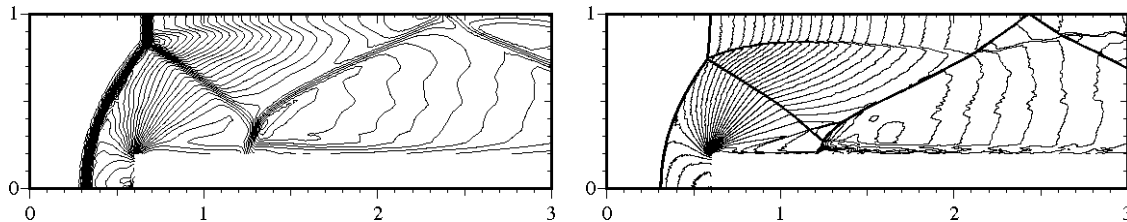


Figure 7: FEM-RK3 solution of the Mach 3 step at  $t = 4$ , density,  $\mathbb{P}_1$  approximation. Left:  $h = 0.25$ , 4813  $\mathbb{P}_1$  nodes. Right:  $h = 0.003$ , 324927  $\mathbb{P}_1$  nodes.

## 5.2 Double Mach reflection

We now solve the so-called double Mach reflection problem at Mach 10. This problem, popularized by Woodward and Colella (see [15] for complete description), involves a Mach 10 shock in air ( $\gamma = 1.4$ ) that impinges a wall with a 60 degree angle. The undisturbed air ahead of the shock has density 1.4 and pressure 1. The computational domain is  $\Omega = (0, 4) \times (0, 1)$ . The reflecting wall lies at the bottom of the domain and starts at  $x = 1/6$ , *i.e.* free slip boundary condition is enforced on  $\{x \geq 1/6, y = 0\}$ . The shock makes a 60 degree angle with the  $x$ -axis. Outflow boundary conditions are enforced at  $\{0 \leq x < 1/6, y = 0\}$  and  $\{x = 4\}$ . The boundary values along the top boundary  $\{y = 1\}$  are set to describe the motion of the initial Mach 10 shock. The flow is computed at time  $t = 0.2$ . The control parameters of the entropy viscosity are  $\alpha_{max} = 0.25$ ,  $\alpha_E = 0.25$ ,  $\mathcal{P} = 0.075$  and  $\mathcal{P}_\rho = 0$ . The tests have been run with  $CFL = 0.5$

We show in Figure 8 the solution computed with  $\mathbb{P}_1$  Lagrange polynomials on a mesh composed of 453969 nodes. The left panel displays the density field in the region  $0 \leq x \leq 3$ . The right panel shows a close up view of the density in the region of the three-shock interaction point. To evaluate the influence of the control parameter  $\alpha_E$  we show in the bottom panel the density field computed with  $\alpha_E = 1$ . The overall features are unchanged but using  $\alpha_E = 1$  slightly smeared the roll-up of the front jet and removed small oscillations.

It is remarkable that the contact discontinuity issuing from the triple point seems quite stable contrary to many published results using high-order methods, see *e.g.* [12, 3]. All these simulations show Kelvin-Helmholtz instabilities developing along the contact line and a jet with almost no roll-up. The present simulation shows instead a jet with a well

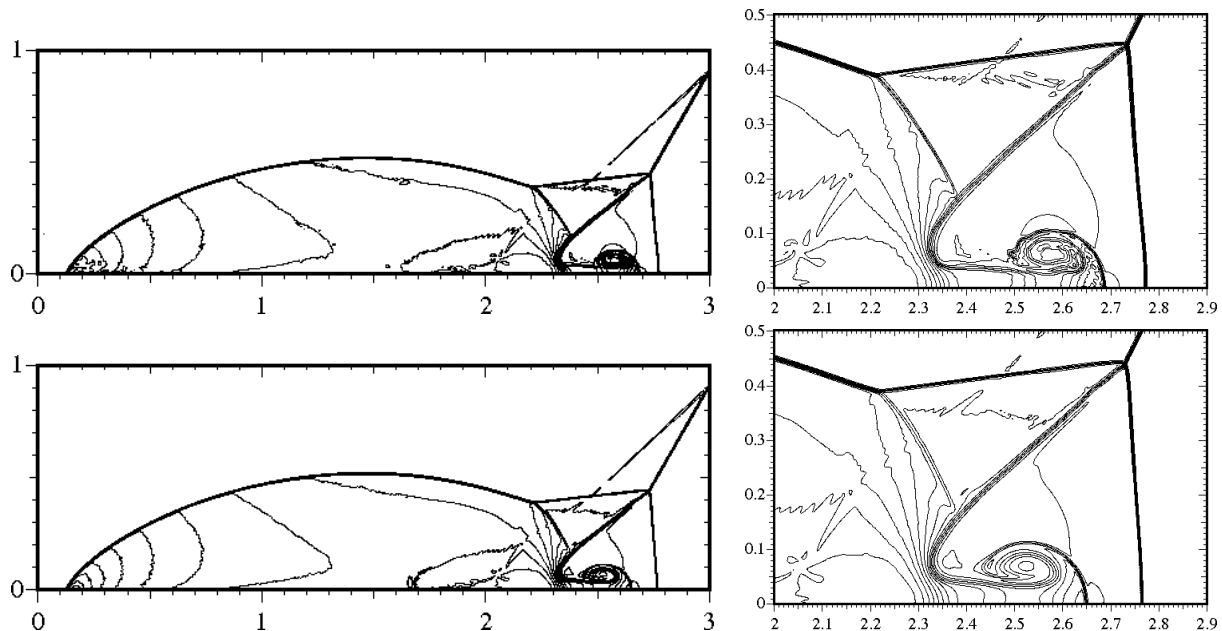


Figure 8: FEM-RK3 solution of the Double Mach reflection at  $t = 0.2$ ,  $M = 10$ , density field, 453969  $\mathbb{P}_1$  nodes. Left: global view. Right: close up view in the region of three-shock interaction point. Top:  $\alpha_E = 0.25$ . Bottom:  $\alpha_E = 1$

developed roll-up but no Kelvin-Helmholtz instabilities along the straight contact line issuing from the triple point. The origin of difference is not clear to us, but a possible explanation is proposed in [2].

### 5.3 Noh problem

We finish this series of tests with the test of Noh [10] for an ideal gas with  $\gamma = 5/3$ . This is a Cauchy problem in  $\mathbb{R}^2$ . The initial data is

$$(\rho, \vec{v}, p) = (1, -(x, y)(x^2 + y^2)^{-1/2}, 0). \quad (15)$$

To avoid singularities when computing the entropy, we set the initial pressure to  $10^{-6}$ . The initial velocity field is circularly symmetric, directed toward the origin with magnitude 1. This problem has an exact solution. It is a circularly symmetric shock reflecting from the origin. The shock speed is  $1/3$ . Behind the shock, *i.e.*  $\sqrt{x^2 + y^2} < \frac{1}{3}t$  the density is 16, the velocity is 0, and the pressure is  $16/3$ . Ahead of the shock, *i.e.* for  $\sqrt{x^2 + y^2} > t/3$ , the density is  $(1 + t/\sqrt{x^2 + y^2})$ , while velocity and pressure are equal to their respective initial value. The computational domain is  $\Omega = (0, 1)^2$ . We use the exact density, pressure, and velocity at the boundaries  $\{x = 1\}$  and  $\{y = 1\}$ . At the other two boundaries  $\{x = 0\}$  and  $\{y = 0\}$  nothing is enforced on  $\rho$  (natural boundary condition), but  $\vec{v} \cdot \vec{n} = 0$  is enforced on the velocity. As reported in [9] most methods dealing with this problem suffer from a very large error in the density at the center.

We have solved this problem with  $\alpha_E = 0.25$ ,  $\mathcal{P}_\rho = 0.025$  and made various tests with  $\mathcal{P} \in \{0.25, 0.5, 1\}$ . The tests have been run with CFL = 0.5 with  $\mathbb{P}_1$  finite elements on a mesh composed 59098 triangles and 29870 nodes,  $h \approx 0.00625$ . The density field at  $t = 2$  is shown in Figure 9. The top panels show the iso-values of the density from 2.5 to 4 with step 0.25 and from 14 to 17 with step 0.2 as done in [9]. The bottom panels show radial profiles of the density field versus radius along nine segments ( $r \in (0, 1), \theta \in \{0, \frac{\pi}{16}, \dots, \frac{7\pi}{16}, \frac{\pi}{2}\}$ ). The results in the left panels have been obtained with  $\mathcal{P} = 1$ , those in the center with  $\mathcal{P} = 0.5$ , and those in the right with  $\mathcal{P} = 0.25$ . These results are comparable with those reported in [9]. It seems that density error at the center decreases as  $\mathcal{P}$  increases.

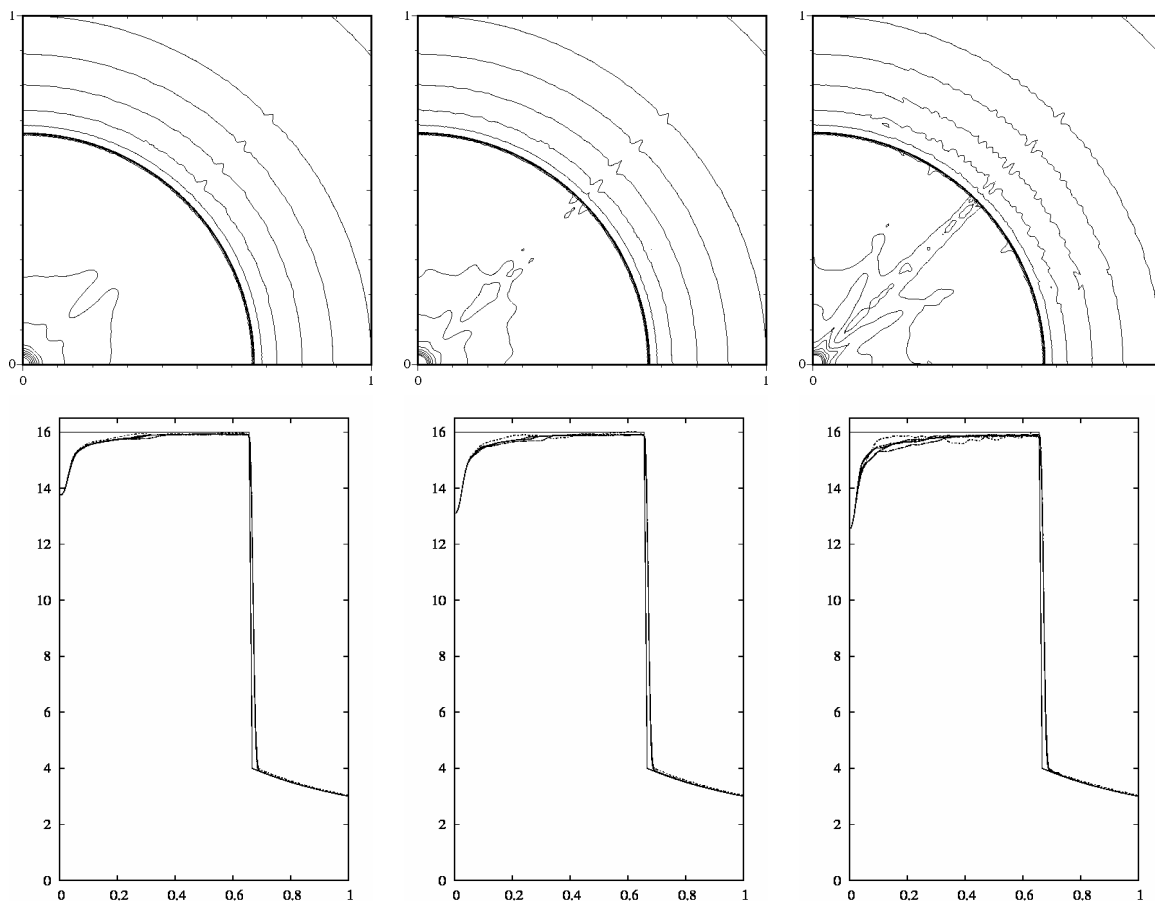


Figure 9: FEM-RK3 solution of the Noh test case at time  $t = 2$ . Top: 23 density contours (from 2.5 to 4 with step 0.25 and from 14 to 17 with step 0.2). Bottom: Density profile versus radius along segments ( $r \in (0, 1), \theta \in \{0, \frac{\pi}{8}, \frac{\pi}{4}, \frac{3\pi}{8}, \frac{\pi}{2}\}$ ). Left panels:  $\mathcal{P} = 1$ . Center panel:  $\mathcal{P} = 0.5$ . Right panel:  $\mathcal{P} = 0.25$ .

The code runs with  $\mathcal{P}_\rho = 0$ , but the density field in the vacuum region develops small oscillations. Using  $\mathcal{P}_\rho = 0.025$  can be viewed as a filtering mechanism for visualization purpose.

## REFERENCES

- [1] A. F. Emery and F. Ashley, An evaluation of several differencing methods for inviscid fluid flow problems, *J. Comput. Phys.*, **2**, 306–331, (1968).
- [2] P. Colella, D. T. Graves, B. J. Keen and D. Modiano, A Cartesian grid embedded boundary method for hyperbolic conservation laws, *J. of Comput. Physics*, **211**, 347 – 366 (2006).
- [3] L. Krivodonova, Limiters for high-order discontinuous Galerkin methods, *J. of Comput. Physics*, **226**, 879 – 896 (2007).
- [4] A. Kurganov, G. Petrova and B. Popov, Adaptive semidiscrete central-upwind schemes for nonconvex hyperbolic conservation laws, *SIAM J. Sci. Comput.*, **29** (6), 1064–8275 (2007).
- [5] J.L. Guermond and R. Pasquetti, Entropy-based nonlinear viscosity for Fourier approximations of conservation laws *C.R. Acad. Sci. Paris*, Ser. I, **346**, 801–806 (2008).
- [6] J.L. Guermond and R. Pasquetti, Entropy viscosity method for high order approximations of stiff problems, ICOSAHOM 09 Congress, Trondheim, June 22-26, 2009.
- [7] J.L. Guermond, R. Pasquetti and B. Popov, Entropy viscosity for nonlinear conservation laws, ENUMATH 09 Congress, Uppsala, June 29 - July 3, 2009.
- [8] R.J. Leveque, Numerical methods for conservation laws, *Lectures in Mathematics, ETH Zürich*, Birkhäuser Verlag, Basel.Boston.Berlin (1992).
- [9] R. Liska and B. Wendroff, Comparison of several difference schemes on 1D and 2D test problems for the Euler equations, *SIAM J. Sci. Comput.*, **25** (3), 995–1017 (2004).
- [10] W.F. Noh, Errors for calculations of strong shocks using an artificial viscosity and artificial heat flux, *J. Comput. Phys.*, **72**, 78–120 (1987).
- [11] P.-O. Persson and J. Peraire, Sub-cell shock capturing for discontinuous Galerkin methods. *AIAA-2006-0112*, Reno, (January 2006).
- [12] J. Shi, Y.-T. Zhang and C.-W. Shu, Resolution of high order WENO schemes for complicated flow structures, *J. of Comput. Physics*, **186**, 690 – 696 (2003).
- [13] E. Tadmor, Convergence of spectral methods for nonlinear conservation laws, *SIAM J. Numer. Anal.*, **26** (1), 30–44 (1989).
- [14] J. Von Neumann and R.D. Richtmayer, A method for the numerical calculation of hydrodynamic shocks, *J. Appl. Phys.*, **21**, 232–237 (1950).

- [15] P. Woodward and P. Colella, The numerical simulation of two-dimensional fluid flow with strong shocks, *J. Comput. Phys.*, **54**, 115–173 (1984).